Air pollutant in East Asia

Makiko Nakata
Faculty of Applied Sociology, Kinki University, Higashi-Osaka 577-8502, Japan
E-Mail: nakata@socio.kindai.ac.jp; Tel: +81-6-6721-2332; Fax: +81-6-6721-2512.

Abstracts

Air pollution in East Asia has become severe in recent years, with heavy air pollutants and Asian dust being transported from China to neighboring countries throughout the year. In this study, we focus on aerosol remote sensing around Beijing, China, in June 2010, when a serious aerosol episode was detected by both satellite and ground measurements. The aerosol model is compiled from the worldwide aerosol monitoring network (NASA/AERONET). We show here that a dense aerosol episode as an example, the air pollution episode around Beijing.

Keywords: aerosol model; Beijing; Biomass burning

1. Introduction

This work is aimed at developing an efficient algorithm for aerosol remote sensing around urban areas in East Asia. The atmospheric aerosol distributions in East Asia are known to be complicated, owing to both natural factors and human activity. In urban areas, small anthropogenic aerosols dominate because of emissions from diesel vehicles and industrial activity. Thee aerosol distribution in East Asia is especially known to be heavily affected by the increasing emissions of sulfuric, nitric, carbonaceous and other aerosols associated with continued economic growth (Kahn et al. 2004). The increasing emissions of anthropogenic particles provide the concentrations of serious air pollutants.

While extreme concentrations of aerosols in the atmosphere can prevent aerosol monitoring with surface-level sun/sky photometers, satellites can still be used in such conditions to observe the Earth's atmosphere from space. It is therefore important to retrieve precise aerosol characteristics from space.

Aerosol distribution varies seasonally because of various factors such as emissions, photochemical reactions and wind direction (Littmann 1991, Kinne et al. 2003). Furthermore, the yellow dust events, which are some of the most dynamic natural phenomena to produce atmospheric aerosols, can increase particulate matter (PM) concentrations and can cause serious atmospheric turbidity (Takemura et al. 2002). Atmospheric aerosols also influence climate because they play an important role in global environmental change (Mukai et al. 2008) and meteorology (Littmann 1991, Pérez et al. 2006). Therefore, it is important to observe aerosol characteristics and their temporal and spatial variations from the ground and from space. Our research group has been working to retrieve aerosol characteristics such as amount, size, composition, and shape based on the combined use of satellite data (Mukai 1990, Mukai et al. 1992), ground measurements (Sano et al. 2003), and numerical model simulations (Mukai et al. 2004).

In this study, we focus on the aerosol characteristics around Beijing, China, during a serious air pollution episode (a dense concentrations of aerosols in the atmosphere) in June, 2010, using simultaneous observations of space-based MODIS sensor products (King et al. 1992) and ground-based Cimel photometer measurements analyzed using a standard AERONET (Aerosol Robotics Network) processing system (Holben et al. 1998, Dubovik and King 2000, Dubovik et al. 2000) that were available to us. This paper is organized as follows. First, the air pollution episode detected at the end of June, 2010 around Beijing based on measurements from space and from the ground is introduced in Section 2. Then, aerosol retrieval algorithms applied to the dense aerosol episode are interpreted, and the retrieved results of aerosol properties around Beijing on June 25, 2010 are shown in Section 3. In Section 4, the retrieved aerosol characteristics are discussed, along with numerical model simulations. Finally, we present a brief summary of our work in Section 5.

2. Aerosol episodes around Beijing

2.1 MODIS Products from space

The Earth-observing MODIS sensor suggests an air

pollution episode around Beijing at the end of June, 2010. Figure 1 presents the Aqua/MODIS products (MYD04_L2 Collection 5.1) around Beijing on June 25, 2010. The left image represents composite image, where a square symbol (□) denotes the AERONET Beijing site (39.97° N, 116.38° E), and small dots represent hot spots, which appear to indicate agricultural biomass burning (Li et al. 2010).

The right image represents the Ångström exponent (α). Aerosol optical thickness (AOT(λ)), where λ represents the wavelength, is the basic parameter describing atmospheric aerosols. The Ångström exponent (α) is derived from the basic data of spectral AOT(λ) as follows (O' Neill et al. 2001);

$$\alpha = - ln (AOT(\lambda 2)/AOT(\lambda 1)) / ln (\lambda 2/ \lambda 1). \quad (1)$$

The values of α are closely related to the aerosol size distribution, e.g., small values of α indicate large particles and large values indicate small particles. In general, values of α from ~0 to 1.0 indicate large particles such as sea salt aerosols and soil dusts, whereas values of $1.0< \alpha <\sim 2.5$ indicate particles such as sulfate and those associated with biomass burning (O' Neill et al. 2003). The aerosol episodes are simply defined as periods of high AOT values. However, each aerosol episode has its own characteristics. Some aerosol episodes show the characteristic features of a dust storm, with a high AOT value and a low α value, but the detection of high α values almost always indicates contamination by small anthropogenic particles.

Assuming values of AOT (0.46 μm) ≥ 4 and $\alpha \geq 1.0$ as the criteria for an aerosol episode of air pollution (Mukai et al. 2012a), the area denoted by a double circle symbol (◎) in Fig. 1 clearly shows an episode of small particle aerosol pollution around Beijing on June 25, 2010. This episode seems to be partly caused by the biomass burnings represented by the dots in the right lower corner in the top images on June 25. This is consistent with almost all of the distribution patterns of aerosol properties in Fig. 1, that show the transportation of dense air parcels from the southeast where agricultural biomass burning usually occurs during this season, to the northwest.

The satellite data should be validated with simultaneous observations from the ground. We examine the ground-based sun photometric data at the Beijing AERONET site in the following.

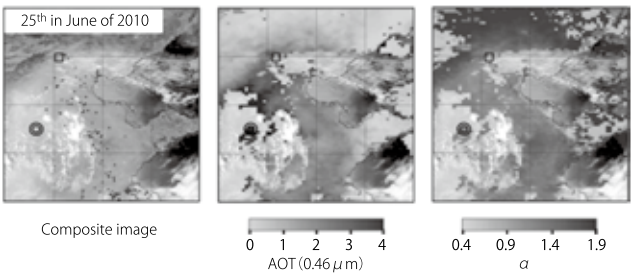

Fig. 1: The figures shows Aqua/MODIS products over Beijing on 25th in June of 2010, where the left, middle and right figures present composite image, AOT distribution and α one (MYD04_L2 Collection 5.1), respectively, and symbol □ indicates the position of AERONET Beijing site and ◎ denotes aerosol retrieval area.

2.2 AERONET measurements from the ground

The worldwide NASA/AERONET data are mostly available as ground-based sun-photometric products. They provide the aerosol optical thickness (AOT(λ)) at wavelength λ. The resolution of the AOT is better than 0.01 in all observation wavelengths and the obtained data are cloud screened before aerosol retrieval (Smirnov et al. 2000). Several other aerosol parameters, such as the Ångström exponent (α) defined by eq.(1), size distribution, refractive index, etc., are derived from the basic data of spectral AOT(λ).

Figure 2 shows these aerosol optical properties (Level-2) observed at the AERONET Beijing site at the end of June, 2010. The top figure (Fig. 2a) shows the aerosol optical thickness at a wavelength of 0.44 μm AOT (0.44). It is clear from eq. (1) that the values of α depend on the wavelength, as seen in Figs. 2b and 2c, where (λ1, λ2) take the values (0.44 μm, 0.675 μm), and (0.675 μm, 0.87 μm), respectively. That is to say, Figs. 2b and 2c represent $\alpha_1 = \alpha_{0.44\text{-}0.675}$ and $\alpha_2 = \alpha_{0.675\text{-}0.87}$. From these figures we find that the two Ångström exponents (α_1, α_2) are different from each other. In order to clarify this, Fig. 2d shows the derivatives of the Ångström exponent (α') (Eck et al. 1999, O' Neill et al. 2001),

$$\alpha' = d\alpha / d \ln \lambda$$
$$= -2 \{ \ln (\tau_{\lambda 3} / \tau_{\lambda 2}) / \ln (\lambda_3 / \lambda_2) - \ln (\tau_{\lambda 2} / \tau_{\lambda 1}) / \ln (\lambda_2 / \lambda_1) \} / \ln(\lambda_3 / \lambda_1). \quad (2)$$

The value of α' appears to indicate the spectral variation of the particle properties. At the very least, the sign of α' appears to signify the particles' properties, i.e., the negative and positive correspond to dry particles and absorbing ones, respectively.

The shaded parts in Fig. 2 represent the simultaneous MODIS observations shown in Fig. 1. The low AOT value on June 24 corresponds to a clear MODIS image, and increasing AOT values on June 25 and 26 indicate the appearance of an

aerosol episode. Ångström exponent (α) values consistently higher than 1.0 in Fig. 2b indicate the existence of small particles around Beijing. The values of α' increase with the AOT values, i.e., low on June 23 and 24, and high from June 25 to 30. This feature of α' suggests the presence of carbonaceous aerosols during the aerosol episode from June 25 to 30. These ground measurements coincide with the satellite observations shown in Fig. 1. In other words, an aerosol episode with small pollutants occurred around Beijing starting June 25, 2010, and carbonaceous aerosols played some role in this episode. Certainly, carbonaceous aerosols come from local sources such as industries and automobiles. However, some appear to be transported from the biomass burning represented by the red dots appeared around the southeastern regions in the top figures of Fig. 1 on June 24 and 25. We test this hypothesis with the retrieved aerosol properties and numerical model simulations in the following section.

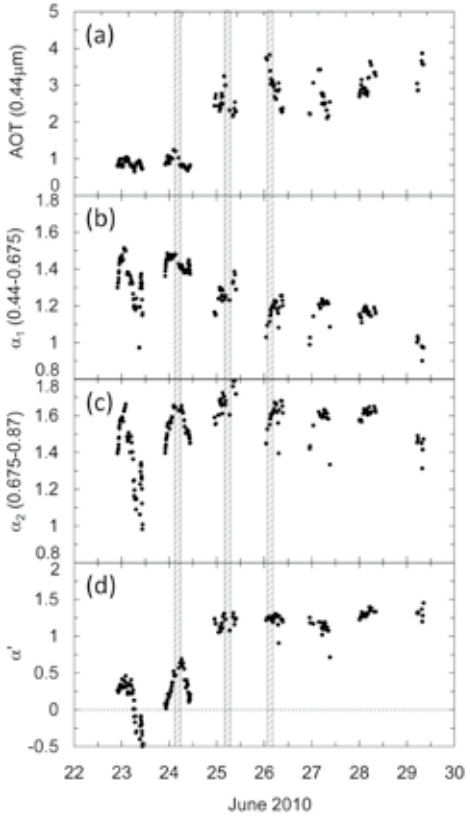

Fig. 2:The AERONET data (Level-2) at AERONET Beijing site on June, 2010. Figs. (a), (b), (c), and (d) represent AOT(0.44 μm), Ångström exponents α_1 and α_2, and derivatives of Ångström exponent (α'), respectively.

3. Algorithms for aerosol retrieval from space

The space-borne sensors measure the upwelling radiance at the top of the atmosphere (TOA), i.e., reflectance (R) from the Earth atmosphere. It is known that incident solar light interacts multiply with atmospheric particles. The multiple scattering calculations (i.e., radiative transfer) take Rayleigh scattering by molecules and Mie scattering by aerosols in the atmosphere into account. In the case of an aerosol episode, we assume an optically semi-infinite atmosphere where radiation incident on the bottom surface is not considered at all. Thus, it is possible to treat only the reflectance R for the semi-infinite case. We propose calculating the reflectance R as a sum of the nth-order of reflection function R^*(n)

$$R = \sum_{n=1}^{\infty} \omega^n R^*(n), \quad (3)$$

where n is the number of times of scattering, and single scattering represents albedo. The nth-order reflection function R^*(n) describes the radiation emerging at the TOA after scattering n times within the atmosphere. This technique is named MSOS (method of successive order of scattering) (Mukai et al. 2012a). The idea of successive scattering is fundamentally related to the probabilistic approach to the theory of radiative transfer. Many papers have been written in this field and much progress has been made. However, since it is beyond the scope of this study to review them all, we refer only to our recent works for the case of a semi-infinite atmosphere (Mukai et al. 2012a & b).

At the first step of radiative transfer, the single scattering behavior of the aerosol model should be determined. We find that the values of high α and negative values of α' suggest that fine-mode anthropogenic aerosols dominate in the atmosphere during the aerosol episode period shown in Figs. 1 and 2 around Beijing. The accumulate AERONET data are used to propose the automatic classification of aerosol observations into 6 categories (DD: Desert Dust, BB: Biomass Burning, RU: Rural, CP: Continental Pollution, PM: Polluted Marine and DP: Dirty Pollution) according to their properties in the global scale (Dubovik et al. 2002, Omar et al. 2005). The data also confirm the consistency and robustness of the method through a cross-validation check. On the other hand, classification with respect to Asian aerosols is also available using the measurements at Asian-AERONET sites as (Ct-1, -2, -3, -4, -5, -6) (Lee et al. 2010). Using these AERONET products on clustering work suggests that the aerosol types treated here roughly correspond to two classes, Continental Pollution (CP) of global classification, and Ct-2 of Asian classification, because these two types mainly contain small anthropogenic pollutants.

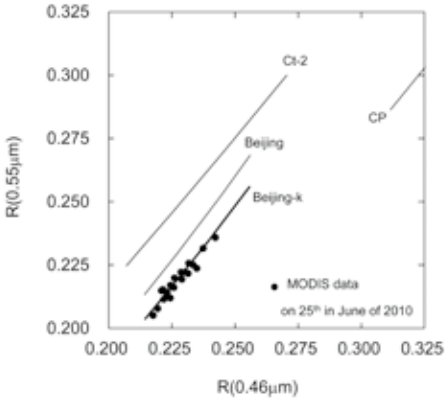

Fig. 3: Simulated values of the reflectance R for aerosol models of CP, Ct-2, Beijing and Beijing-k (refer to Table 1) in a two-channel diagram at wavelengths of 0.46 μm and 0.55 μm. The black filled circles denote MODIS data on June 25, 2010.

Some Aqua/MODIS data from June 25, 2010, from the area indicated by double circles (◎) in Fig. 1, are examined here for aerosol retrieval. The black filled circles in Fig. 3 represent these MODIS data. The solid curves in Fig. 3 show the simulated values of the reflectance R based on the calculation with MSOS in a two-channel diagram with wavelengths of 0.46 μm and 0.55 μm. The atmosphere consists of the above mentioned aerosol types (CP and Ct-2), an aerosol model obtained at Beijing AERONET site, and the Beijing-k aerosol type, which is a modified version of the Beijing type, with slightly stronger absorbing particles (Fuller et al. 1999). The aerosol parameters in our present calculations are size distribution, which is represented by the fine particle fraction, and refractive indices, which are provided in Table 1. Table 1 presents the values of complex refractive indices, $m(\lambda) = n(\lambda) - k(\lambda)\,i$, adopted as aerosol properties for the calculations of reflectance R in Fig. 3 .

Aerosol types	Complex refractive indices ($m(\lambda)=n(\lambda)-k(\lambda)\,i$)			
	0.46(μm)		0.55(μm)	
	n	k	n	k
CP	1.415	0.006	1.410	0.006
Ct-2	1.479	0.010	1.480	0.009
Beijing	1.491	0.014	1.492	0.013
Bejing-k	1.491	0.014	1.492	0.014

Table 1: Complex refractive indices; $m(\lambda)=n(\lambda)-k(\lambda)\,i$, where λ represents wavelength, for CP, Ct-2 aerosol types, and Beijing AERONET site and Beijing-k aerosol types (refer to Fig. 3).

Figure 3 shows that the Beijing-k type aerosol is consistent with the MODIS data. Furthermore, we can rank the retrieved aerosols according to their fit to the June 25, 2010 MODIS data around Beijing, from best to worst:

1) Beijing-k type
2) Beijing type
3) Ct-2 type in Asian
4) CP type in global clustering

The reflectance values obtained using the CP type aerosol are too high compared to MODIS data, therefore CP type aerosols do not explain this Beijing aerosol episode. We therefore conclude that the Asian regional type (Ct-2) aerosol is a better fit than the global (CP) type aerosol, and furthermore, the local Beijing aerosol type is a much better fit for interpret the local observations. These results seem reasonable, suggesting that detailed measurements in both spatial and temporal scales are necessary for precise analysis of aerosols.

The best candidate Beijing-k type aerosol suggests the inclusion of carbonaceous aerosols. Transportation of biomass burning aerosols (Li et al. 2010, Xue et al. 2012) is observed in the satellite images in Fig. 1 on June 24 and 25, where carbonaceous aerosols appear to be transported from the southwest toward Beijing.

4. Discussions based on numerical model simulations

Figure 4 shows the simulated distribution of each AOT component relative to the total AOT in East Asia on June 25, 2010. We use the three-dimensional aerosol-transport-radiation model SPRINTARS (Takemura et al. 2005) to model carbonaceous, sulfate, dust, and sea salt aerosols. Figs. 4a and 4b represent the ratio of AOT (0.55 μm) of sulfate and carbonaceous components to the total AOT, respectively. Fig. 4a shows that sulfate dominates all over East Asia, and Fig. 4b shows that the carbonaceous component is concentrated in the south. Fig. 5 shows the contribution of the aerosol components to the simulated AOT for the Beijing AERONET site (39.97° N, 116.38° E) and MODIS reference area (37.06° N, 115.35° E) for aerosol retrieval.

The sulfate component is dominant in both graphs in Fig. 5, consistent with Fig. 4a. As for the carbonaceous component, the value in the reference area is slightly larger than at the Beijing site. This simulation result supports the hypothesis that the Beijing-k aerosol type, which is the best candidate to interpret MODIS data in Fig. 3, is a stronger absorber than the Beijing type (refer to Table 1), and seems to suggest that some of the carbonaceous aerosols are transported from the southeast toward Beijing. Of course, the carbonaceous aerosols emanate from local industries or automobiles. However, only in the case of local emissions, the emission volumes in urban cities such as Beijing are higher than those in remote rural areas such as the reference areas shown for aerosol retrieval in this work (Fig. 3).

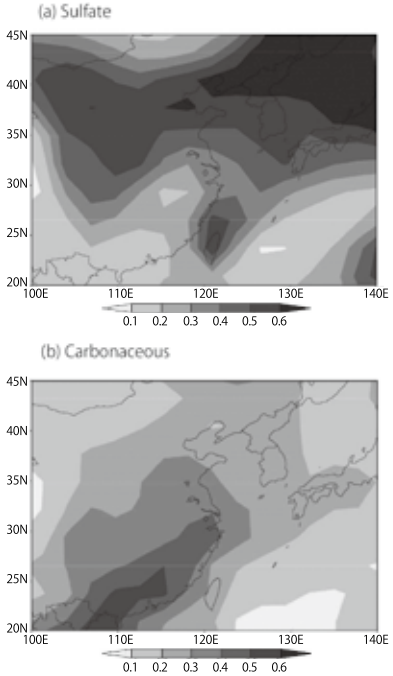

Fig. 4: Distribution of ratios of simulated (a) sulfate AOT and (b) carbonaceous AOT components relative to the total AOT at a wavelength of 0.55 μm in East Asia on June 25, 2010.

5. Summary

In this work we focus on aerosol characteristics during serious aerosol episodes (dense concentrations of aerosols in the atmosphere), detected by both satellite and ground measurements in East Asia.

We show that dense aerosol episodes can be well simulated using a semi-infinite radiative transfer model composed of Rayleigh scattering by molecules and Mie scattering by proposed aerosol types, which are compiled from the accumulated measurements provided by the worldwide aerosol monitoring network (NASA/AERONET). In addition, the efficient procedure for solving the radiative transfer problem for semi-infinite medium named MSOS (Method of Successive Order of Scattering) is applied for Aqua/MODIS data around Beijing.

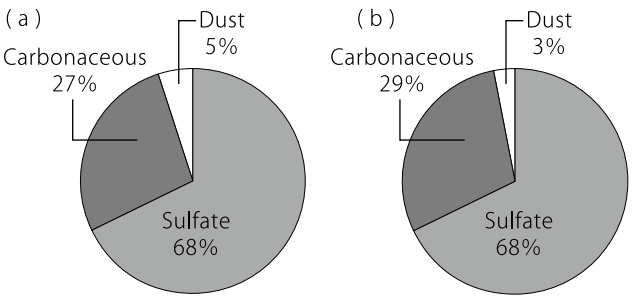

Fig. 5: AOT contribution (%) of each component relative to total particles at (a) Beijing AERONET site (39.97° N, 116.38° E), and (b) the reference area (37.06° N, 115.35° E) (refer to Figs. 3 and 4).

We conclude that air pollution over Beijing is mainly due to both the increasing emissions of the anthropogenic aerosols associated with economic growth and the complicated behavior of natural dust. However, carbonaceous aerosols from agriculture biomass burning in Southeast Asia also contribute to the pollution. Air quality is worse in big cities than in remote areas, therefore high resolution measurements of atmospheric aerosols in spatial- and temporal- scales are needed in Asian urban cities such as Beijing.

Acknowledgements

The author thanks the REESIT members for their helpful suggestions and discussions, and NASA for distributing the MODIS data and the AERONET team for data processing. This work was supported in part by Global Change Observation Mission—Climate (GCOM-C) by JAXA (no. JX-PSPC-308878).

References

Dubovik, O., Smirnov, A., Holben, B.N., King, M.D., Kaufman, Y.J., Eck, T.F., 2000. Slutsker, I. Accuracy assessments of aerosol optical properties retrieved from AERONET sun and sky-radiaometric measurements. J. Geophys. Res. 105, 9791–9806.

Dubovik, O., King, M.D., 2000. A flexible inversion algorithm for retrieval of aerosols optical properties from sun and sky radiance measurements. J. Geophys. Res. 105, 20673–20696.

Dubovik, O., Holben, B.N., Eck, T.F., Smirnov, A., Kaufman, Y.J., King, M.D.,Tanré, D. and Slutsker, I., 2002. Variability of absorption and optical properties of key aerosol types observed in worldwide locations, J. Atmos. Sci. 59, 590–608.

Eck, T.F., Holben, B.N., Reid, J.S., Dubovik, O., Smirnov, A., O'Neill, N.T., Slutsker, I., Kinne, S., 1999. Wavelength dependence of the optical depth of biomass burning, urban, and desert dust aerosols. J. Geophys. Res. 104, 31,333–31,349.

Fuller, Kirk A., Malm, William C. Kreidenweis, Sonia M., 1999. Effects of mixing on extinction by carbonaceous particles, J. Geophys. Res. 104, D13, 15941-15954.

Holben, B.N., Eck, T.F., Slutsker, I., Tanre, D., Buis, J.P., Setzer, A., Vermote, E., Reagan, J.A., Kaufman, Y., Nakajima, T., 1998. AERONET-A federated instrument network and data archive for aerosol characterization. Rem. Sens. Environ. 66, 1–16.

Kahn, R., Anderson, J., Anderson, T.L., Bates, T., Brechtel, F., Carrico, C.M., Clarke, A., Doherty, S.J., Dutton, E., Flagan, R., 2004. Environmental snapshots from ACE-Asia. J. Geophys. Res. 109, D19S14, doi:10.1029/2003JD004339.

King, M.D., Kaufman, Y.J., Menzel, W.P. and Tanré, D., 1992. Remote sensing of cloud, aerosol, and water vapor properties from the Moderate Resolution Imaging Spectrometer (MODIS), IEEE Trans. Geosci. Remote Sensing 30, 2–27.

Kinne, S., Lohmann, U., Feichter, J., Schulz, M., Timmreck, C., Ghan, S., Easter, R., Chin, M., Ginoux, P., Takemura, T., 2003. Monthly averages of aerosol properties: A global comparison among models, satellite data, and AERONET ground data. J. Geophys. Res. 108, D20, doi:10.1029/2001JD001253.

Lee, K.H. and Kim, Y. J., 2010. Satellite remote sensing of Asian aerosols: a case study of clean, polluted and dust storm days, Atmos. Meas. Tech. Discuss. 3, 2651–2680.

Li, W.J., Shao, L.Y., Buseck, P.R., 2010. Haze types in Beijing and the influence of agricultural biomass burning, Atmos. Chem. Phys. 10, 8119-8130.

Littmann, T., 1991. Dust storm frequency in Asia: Climatic control and variability. Int. J. Climatol. 11, 393–412.

Mukai, S., 1990. Atmospheric correction of remote sensing images of the ocean based on multiple scattering calculations. IEEE Trans. Geosci. Remote Sensing, 28, 696–702.

Mukai, S., Sano, I., Masuda, K., Takashima, T., 1992. Atmospheric correction for ocean color remote sensing: Optical properties of aerosols derived from CZCS imagery. IEEE Trans. Geosci. Remote Sens. 30, 818–824.

Mukai (Nakata), M., Nakajima, T. and Takemura, T., 2004. A study of long-term trends in mineral dust aerosol distributions in Asia using a general circulation model. J. Geophys. Res. 109, D19204.

Mukai (Nakata), M., Nakajima, T., Takemura, T. 2008. A study of anthropogenic impacts of the radiation budget and the cloud field in East Asia based on model simulations with GCM. J. Geophys. Res. 113, D12211, doi:10.1029/2007JD009325.

Mukai, S., Yokomae, T., Sano, I., Nakata, M. and Kohkanovsky, A. 2012a. Multiple scattering in a dense aerosol atmosphere, Atmos. Meas. Tech. Discuss. 5, 881-907.

Mukai, S., Sano, I. and Nakata, M., 2012b. Algorithms for radiative transfer simulations for aerosol retrieval, Proc. of SPIE, 8534, Remote Sensing of Clouds and the Atmosphere XVII, and Lidar Technologies, Techniques, and Measurements for Atmospheric Remote Sensing VIII 85340T, doi:10.1117/12.974430.

Omar, A.H., Won, J.-G., Winker, D.M., Yoon, S.-C., Dubovik, O., McCormick, M.P., 2005. Development of global aerosol models using cluster analysis of Aerosol Robotic Network (AERONET) measurements. J. Geophys. Res. 110, doi:10.1029/2004JD004874.

O'Neill, N.T., Dubovik, O., Eck, T.F., 2001. Modified Angstrom exponent for the characterization of submicrometer aerosols, Appl. Optics 40, 2368-2375.

O'Neill, N.T., Eck, T.F., Smirnov, A., Holben, B.N., Thulasiraman, S., 2003. Spectral discrimination of coarse and fine mode optical depth, J. Geophys. Res. 108, 4559, doi:10.1029/2002JD0029753.

Pérez, C., Nickovic, S., Pejanovic, G., Baldasano, J.M., Özsoy, E., 2006. Interactive dust-radiation modeling: A step to improve weather forecast. J. Geophys Res. 111, D16206.

Sano, I., Mukai, S., Okada, Y., Holben, B.N., Ohta, S., Takamura, T., 2003. Optical properties of aerosols during APEX and ACE-Asia experiments. J. Geophys Res. 108, 8649.

Smirnov, A., Holben, B.N., Eck, T.F., Dubovik, O., 2000. Slutsker, I. Cloud screening and quality control algorithms for the AERONET database. Remote Sens. Environ. 73, 337–349.

Takemura, T., Uno, I., Nakajima, T., Higurashi, A., Sano, I., 2002. Modeling study of long-range transport of Asian dust and anthropogenic aerosols from Asia. Geophys. Res. Lett. 29, 2158, doi:10.1029/2002GL016251.12, 10461-10492.

Takemura, T., Nozawa, T., Emori, S., Nakajima, T.Y., Nakajima, T., 2005. Simulation of climate response to aerosol direct and indirect effects with aerosol transport-radiation model. J. Geophys. Res. 110, doi:10.1029/2004JD005029.

Xue, Y., Xu, H., Mei, L., Guang, J., Guo, J., Li, Y., Hou, T., Li, C.,Yang L., He, X., 2012. Merging aerosol optical depth data from multiple scattering missions to view agricultural biomass burning in central and East China., Atmos. Chem. Phys. Discuss.

Makiko Nakata

Assistant Professor, Dr. Sci.
Kinki University, Faculty of Applied Sociology.
3-4-1 Kowakae, Higashi-Osaka, 577-8502, Japan